AIAA JOURNAL
Vol. 44, No. 3, March 2006

Dynamic Stall Flow Control via a Trailing-Edge Flap

P. Gerontakos* and T. Lee†
McGill University, Montreal, Quebec H3A 2K6, Canada

Effects of a moveable trailing-edge flap on the dynamic-load loops of an oscillating NACA 0015 airfoil were investigated at $Re = 1.65 \times 10^5$. Both upward and downward flap deflections for different flap actuation start times, durations, and amplitudes were considered. Surface pressure measurements show that only upward flap deflections led to the reduction of nose-down pitching moment, and that the larger the flap deflection the more efficient the reduction mechanism was. The shorter the actuation duration the smaller the poststall lift loss. The reduction of the peak nose-down pitching moment was a consequence of the suction pressure appearing on the lower surface of the trailing-edge flap. The formation and detachment of the dynamic-stall vortex was not affected by the flap motion, whereas the low-pressure signature of the vortex was reduced by the upward flap deflection. The later the flap actuation during the upstroke, the greater the net torsional damping was. Optimum flap motion is also discussed.

Nomenclature

C_d	=	section drag coefficient
C_l	=	section lift coefficient
C_m	=	section pitching moment coefficient about quarter chord
C_w	=	torsional damping factor
c	=	airfoil chord
f_o	=	oscillation frequency
Re	=	Reynolds number, $= u_\infty c/\nu$
t	=	time
t_d	=	flap actuation duration
t'_d	=	nondimensional t_d, $= t_d u_\infty/c$
t_e	=	end of flap actuation
t'_e	=	nondimensional t_e, $= t_e u_\infty/c$
t_s	=	flap actuation start time
t'_s	=	nondimensional t_s, $= t_s u_\infty/c$
t_{ss}	=	steady-state time period
u	=	mean wake velocity
u'	=	streamwise wake velocity fluctuation
u_∞	=	freestream velocity
x	=	streamwise distance
y	=	normal distance
α	=	angle of attack
α_{ds}	=	dynamic stall angle
α_m	=	mean angle of attack
α_{ms}	=	moment stall angle
α_{ss}	=	static stall angle
$\Delta\alpha$	=	oscillation amplitude
δ_{max}	=	maximum flap deflection
κ	=	reduced frequency, $= \omega c/2u_\infty$
ν	=	kinematic viscosity
ω	=	oscillatory radian frequency, $= 2\pi f_o$

Subscript

u	=	pitch-up
d	=	pitch-down

Received 21 April 2005; revision received 15 August 2005; accepted for publication 22 August 2005.

*Graduate Research Assistant, Department of Mechanical Engineering.
†Associate Professor, Department of Mechanical Engineering. Member AIAA.

I. Introduction

DYNAMIC overshoots in lift and drag forces and accompanying high torsional and pitch control loads on helicopter rotor blades continue to make dynamic stall and its control an important topic in rotorcraft engineering. Numerous experimental and computational investigations[1−6] have been conducted to investigate and understand dynamic stall flow phenomena under the influence of different oscillation frequencies and amplitudes. It is now known that the predominant feature of dynamic stall is the formation, convection, and shedding over the upper surface of the airfoil of an energetic leading-edge vortex (LEV), or dynamic stall vortex, which induces a nonlinearly fluctuating pressure field and produces large transient variations in forces and moments that may be many times larger than their static counterparts. Rapid downstream convection of the LEV acts to enhance the lift being produced and also produces a rapid aft movement of the center of pressure, which results in large nose-down pitching moments on the airfoil section and an increase in torsional loads of the blades. This is the main adverse characteristic of dynamic stall that concerns helicopter dynamicists. Moreover, once the LEV passes the airfoil trailing edge and moves into the wake, the flow progresses to a state of poststall full separation over the upper surface and an abrupt loss of lift is incurred. Also, if and when the angle of attack becomes low enough during the pitch-down motion, the flow will finally reattach again from the leading edge. An excellent review of unsteady airfoils is given by McCroskey.[3]

A number of passive and active dynamic-stall flow-control concepts, such as the use of a trailing-edge flap,[7−11] pulsating and synthetic jets,[12−14] leading-edge blowing and suction,[15,16] leading-edge rotating cylinder,[17] and dynamically deformable or variable droop leading edge,[18,19] capable of minimizing, or eliminating, detrimental hysteresis in nonlinear airloads and aerodynamic damping have been proposed. Note that depending on the application, the objectives of dynamic-flow control could be very different. In helicopter applications, the objective is to prevent LEV occurrence and, subsequently, the undesirable increase in the nose-down pitching moment on rotor blades. For highly maneuverable aircraft, however, the purpose is to utilize the increased dynamic lift via the delay of LEV detachment from the airfoil suction surface. Nevertheless, active flow-control schemes show the most promise, because the flow-control device can be designed to affect the flow only on the retreating side, without compromising the performance of the blade on the advancing side. Among them, the trailing-edge flap (TEF) flow-control techniques have been examined both experimentally and computationally[7−11] by researchers elsewhere. The TEF dynamic flow control concept is presumed to be more applicable, considering the severe environment frequently encountered at the leading edge of a rotor blade.

Trailing-edge flaps have been used extensively as a routine method of controlling lift by temporarily altering airfoil camber on an airplane in steady low-speed operations, especially during takeoff and landing, without penalizing cruise performance. More recently, trailing-edge flaps have been used as unsteady aerodynamic control devices for the control of transient lift on maneuvering fighter aircraft and large negative pitch moment on helicopter rotor blades, as well as in an attempt to control unsteady lift, including flutter suppression and gust alleviation. Airfoil lift characteristics for unsteady trailing-edge flap motions were first analyzed by Theodorsen[20] for harmonically oscillating flaps. Most recently, Feszty et al.[11] reported computationally that the pitching-moment loads associated with the dynamic stall occurring on an oscillating NACA 0012 airfoil could be reduced by the use of a pulsed trailing-edge flap. The wing model was equipped with a 16% chord flap and was oscillated sinusoidally with $\alpha(t) = 15\text{ deg} + 10\text{ deg}\sin\omega t$ at a reduced frequency of 0.173 and $Re = 1.463 \times 10^6$. Feszty et al.'s computational fluid dynamics results suggested that a trailing-edge vortex (TEV), induced by the downstream convecting LEV, was in fact responsible for the large negative pitch-moment coefficient C_m and the associated negative damping. They also suggested that optimum pulsed TEF motions, represented by $\delta(t) = \delta_{\max}[1 - \cos(t/t_d)]$, with an upward flap deflection of $\delta_{\max} = 20$ deg, a flap duration of about $\frac{1}{3}$ of the airfoil motion time period, and a start time in the third quarter of the azimuth should be applied to displace the TEV and effectively modify the LEV trajectory. However, despite much predictive work, published experimental data on the unsteady aerodynamic loads of dynamically deflecting control surfaces are sparse.

The objective of the current work was to investigate the control of the dynamic airloads on a sinusoidally oscillating NACA 0015 airfoil via a movable trailing-edge flap (TEF) in a subsonic wind tunnel. Special emphasis was placed on simultaneous measurements of airfoil and flap deflection histories, synchronized with detailed surface-pressure measurements. The dynamic airloads were then obtained by integrating the unsteady surface pressures measured at a finite number of locations on the airfoil surface. Cross-hot-wire wake measurements were also made to supplement the surface-pressure results. The experiments were divided into two parts. In the first part, the dynamic load loops of an oscillating baseline airfoil, at selected oscillation frequencies and amplitudes, with no TEF flow control were investigated. The static-airfoil data were also obtained for comparison. In the second part, the effects of TEF actuation duration, deflection amplitude $\delta_{\max}$, and start time on the dynamic C_l–C_d–C_m curves were characterized. Both upward and downward flap deflections were tested, and optimum TEF control schemes are discussed.

II. Experimental Methods

The experiment was conducted in the recently constructed $0.9 \times 1.2 \times 2.7$ m low-speed suction-type wind tunnel at McGill University with a freestream turbulence intensity of 0.03% at $u_\infty = 35$ m/s. A rectangular, untwisted NACA 0015 airfoil, fabricated from solid aluminum, with a chord length c of 25.4 cm and a span b of 38 cm, was used as the test model. The wing model was mounted horizontally at the center of the wind tunnel test section. Two 40-cm-diam aluminum endplates with sharp leading edges were fixed to each end support, located 41 cm from the sidewall of the test section. The gap between the wing and the endplate was kept at less than 1 mm to minimize the leakage flow through the gap. The origin of the coordinate was located at the leading edge of the airfoil with x, y, and z in the streamwise, normal, and spanwise directions, respectively. The two-dimensional uniformity of the flow distribution over the airfoil model was checked by traversing a 5-μm normal hot-wire probe located at 30%c downstream from the leading edge of the airfoil and $y = 5$ mm above the airfoil. The nonuniformity was found to be ±3% of the freestream value. The freestream velocity u_∞ was fixed at 10.1 m/s, which yielded a chord Reynolds number of 1.65×10^5.

The wing was equipped with a full-span trailing-edge-flap flow-control system. A 25%c trailing-edge flap of a simple hinged type was activated and deactivated independently by a Futaba Model S-3003 servomotor located at the wing root and driven by a custom-built controller (Fig. 1a), which actuated the flap in response to the wing phase signal. Trailing-edge flap actuation employed a brief pulse and was actuated at any desired time and instantaneous angle of attack. The pulse signal was represented by a constant ramp-up motion, remained steady briefly, and was followed by a constant ramp-down motion (Fig. 1b). Actuation duration t_d, amplitude $\delta_{\max}$, and start time t_s were tested independently first to quantify their effects on the dynamic-stall lift and pitching-moment loads and the wake flow structure. These results then served as an experimental guideline for optimum control of detrimental-dynamic stall hysteresis effects. Both upward and downward flap deflections with $\delta_{\max} = \pm 7.5$ deg and ±15 deg were tested. It is noteworthy that the TEF motions tested to control the unsteady lift and pitching moment were determined based on the uncontrolled baseline dynamic $-C_l$ and $-C_m$ loops, as shown in Fig. 2, as well as on the spatial–temporal progression of the unsteady boundary-layer and stall events observed on an oscillating NACA 0012 airfoil.[6] The flap actuation start times $t_s = -0.5\pi$, 0π, and 0.5π radians were chosen to correspond to the angles of attack at the beginning of pitch-up, the beginning of upstream movement of the flow reversal, and the end of pitch-up motion, respectively.

A specially designed four-bar linkage and flywheel oscillation mechanism, capable of oscillating the airfoil sinusoidally at various amplitudes and frequencies, mounted externally on the wind tunnel was used in the present experiment (Fig. 1a). The oscillating airfoil was chosen to simulate the quasi-periodic first harmonic angle-of-attack variations that are found on helicopter rotors during low-speed forward flight. Mean angle of attack α_m was varied by changing the relative angle between the rotating shaft and the rocker–shaft connector. Oscillation amplitude $\Delta\alpha$ was varied by attaching the coupler at specific radial locations on the flywheel. The flywheel was attached directly to an Exlar Model DXM340C servomotor driven by an Emerson Model FX3161 PCM1 programmable motion controller. Oscillation frequency was monitored in real time using an HP Model 3581A spectral analyzer and was measured to an accuracy of ±0.02 Hz. The four-bar mechanism provided an output that was sinusoidal to within 2%. The airfoil pitch axis was located at the quarter chord location. The instantaneous angle of attack $\alpha(t)$ of the airfoil and the phase reference signal were recorded from both the servomotor feedback resolver and a potentiometer mounted on the servomotor shaft. For the TEF control experiment, the airfoil was oscillated through the static-stall angle $\alpha_{ss} = 16.5$ deg with $\alpha(t) = 15\text{ deg} + 10\text{ deg}\sin\omega t$ (where $\omega = 2\pi f_o$, f_o is the oscillation frequency, and t is the time) and a reduced frequency $\kappa(= \omega c/2u_\infty)$ of 0.05. Also, in the following discussion, the suffix u is used to indicate pitch-up when α is increasing and d is used to indicate pitch-down when α is decreasing.

Surface pressure distributions were obtained from 48 0.35-mm-diam pressure taps, covering up to $x/c = 96.3\%$, distributed over the upper and lower surfaces of the wing model (Fig. 1c). The orifices, located along the midspan of the airfoil, were staggered 1.5 mm apart in the spanwise direction to avoid the wake effect from an upstream orifice on orifices farther downstream. Pressure signals, recorded using a fast-response Honeywell DRAL501 differential pressure transducer (with a range of 50 mm of water head) connected via a 48-port scanivalve system, were phase-locked ensemble-averaged over 75 cycles of oscillation and were integrated numerically to compute the unsteady aerodynamic loads and pitching moments. The dynamic range of the pressure transducer was on the order of 10 kHz. The transducer signals were low-pass filtered (250 Hz) and amplified with a multichannel AA Lab Model G3006 pressure measurement system. The effects of the 35-cm-long and 0.75-mm-i.d. plastic tubing, separating the surface tap and the pressure transducer, on the unsteady pressure signals were examined by comparing the transducer output level and the phase with a controlled acoustic sound source. The effect of the length of the plastic tubing was found to be a simple time constant delay on all pressure signals with frequency above 2.95 Hz, which yielded a limited reduced frequency κ of 0.233 at $u_\infty = 10.1$ m/s or $Re = 1.65 \times 10^5$ in the present experiment. Details of this method can be found in

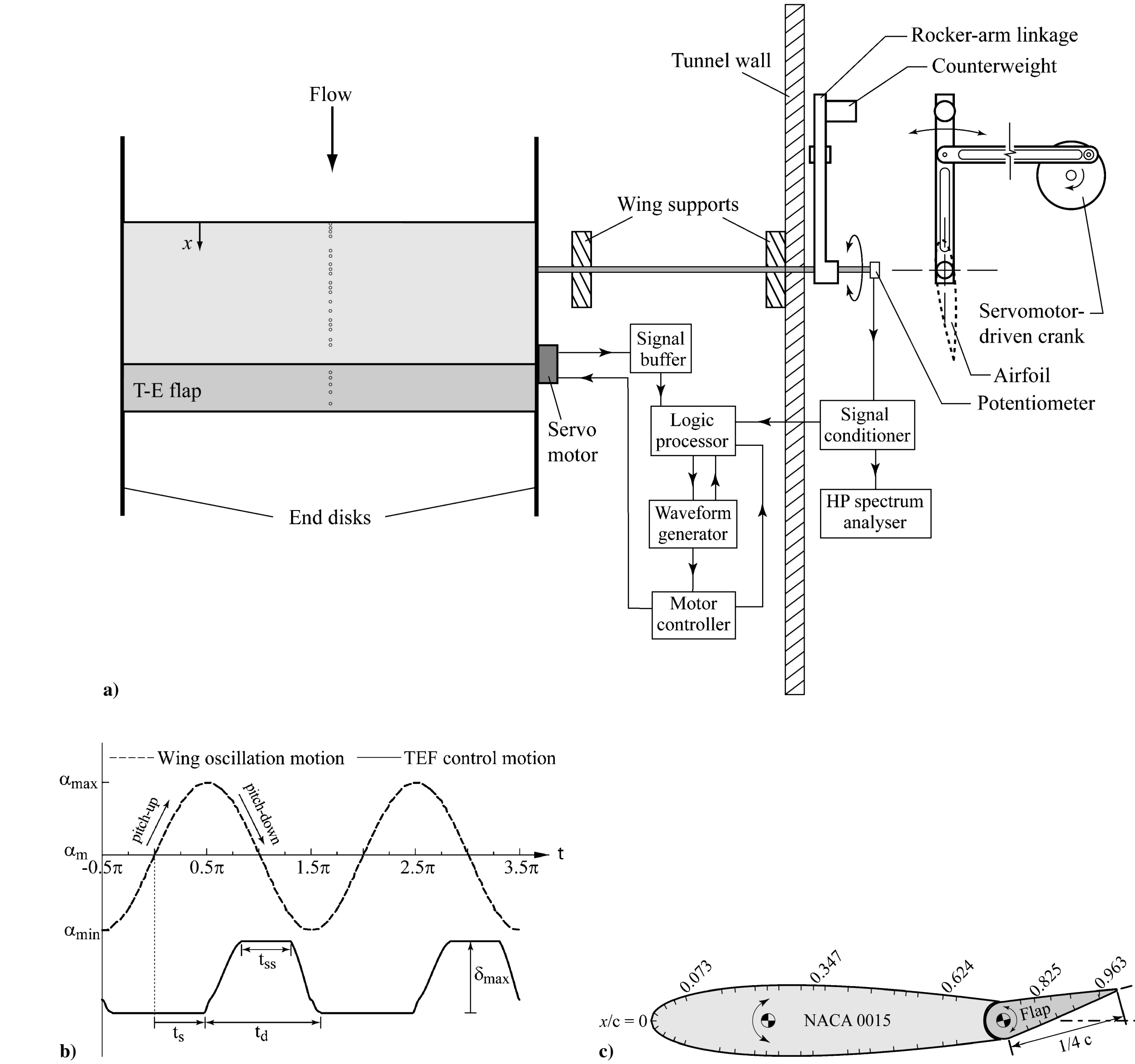

Fig. 1 Experimental setup: a) schematics of wing model and experimental setup; b) definition of flap actuation start time t_s, duration t_d, and amplitude $\delta_{\max}$; and c) surface pressure tap locations.

the work of Lee and Basu[5] and Rennie and Jumper.[7] Uncertainty analysis gives a typical total uncertainty of ± 0.013 in C_p.

The wake of the airfoil model was examined using a miniature cross-hot-wire probe with two Dantec 56C17 constant-temperature anemometers. The overheat ratio was set at 1.6. The hot-wire probe was mounted on a sting extended from a computer-controlled three-dimensional traversing mechanism and was located one chord downstream of the trailing edge of the airfoil. All hot-wire calibrations, mean-flow measurements, freestream turbulence levels, rms disturbance measurements, and subsequent processing were performed on a Pentium III PC with a 16-bit A/D converter board. The hot-wire signals were sampled at 2 kHz. Instantaneous wake velocities were subsequently ensemble-averaged over a large number of oscillation cycles to obtain the phase-locked average of the mean and fluctuating velocity fields at various phase positions during the oscillation cycle.

III. Results and Discussion

A. Baseline Wing

The dynamic C_l and C_m loops of a NACA 0015 airfoil oscillated with $\alpha_m = 10$, 12.5, and 15 deg at fixed $\Delta\alpha = 10$ deg and $\kappa = 0.05$ are presented in Figs. 2a–2d. Also shown in Fig. 2a is the C_l–α curve of a NACA 0012 airfoil oscillated well beyond $\alpha_{ss} = 13$ deg with $\alpha_m = 10$ deg, $\Delta\alpha = 10$ deg, and $\kappa = 0.05$. Figure 2a shows that for NACA 0015 airfoil oscillating with $\alpha(t) = 15$ deg $+ 10$ deg $\sin\omega t$ and $\kappa = 0.05$, the dynamic maximum lift coefficient $C_{l,\max}$ (at $\alpha_{ds} = 22.1$ deg) was about 0.32 higher than the static stall value (at $\alpha_{ss} = 16.5$ deg), but the large nose-down pitching moment was of more significance. A 6.3 times increase in $|-C_{m,\text{peak}}|$ was observed. It is of interest to note that there was a double peak in the lift coefficient prior to the dynamic-stall angle α_{ds}. The presence of the double peak was somewhat unexpected as compared to the single peak presented in the dynamic C_l loop of an oscillating NACA 0012 airfoil (denoted by the $\cdots$ line in Fig. 2a). This rather unusual sequence of dynamic stall events can be explained from a careful examination of the surface pressure coefficient C_p distributions on both the NACA 0015 and 0012 airfoils, as shown in Fig. 3. Figure 3a suggests that for an oscillating NACA 0015 airfoil, the upstream movement of the turbulent boundary-layer breakdown, or separation (at $\alpha_u \approx 19.3$ deg), was somewhat prolonged and sluggish, compared to a NACA 0012 airfoil[6] (Fig. 3b), before the formation and detachment of a LEV from the wing upper surface (at $\alpha_u \approx 20.9$ deg). Note that for a NACA 0012 airfoil oscillating with $\alpha(t) = 10$ deg $+ 10$ deg $\sin\omega t$, the dynamic stall mechanism was characterized by the sudden breakdown of the turbulent boundary

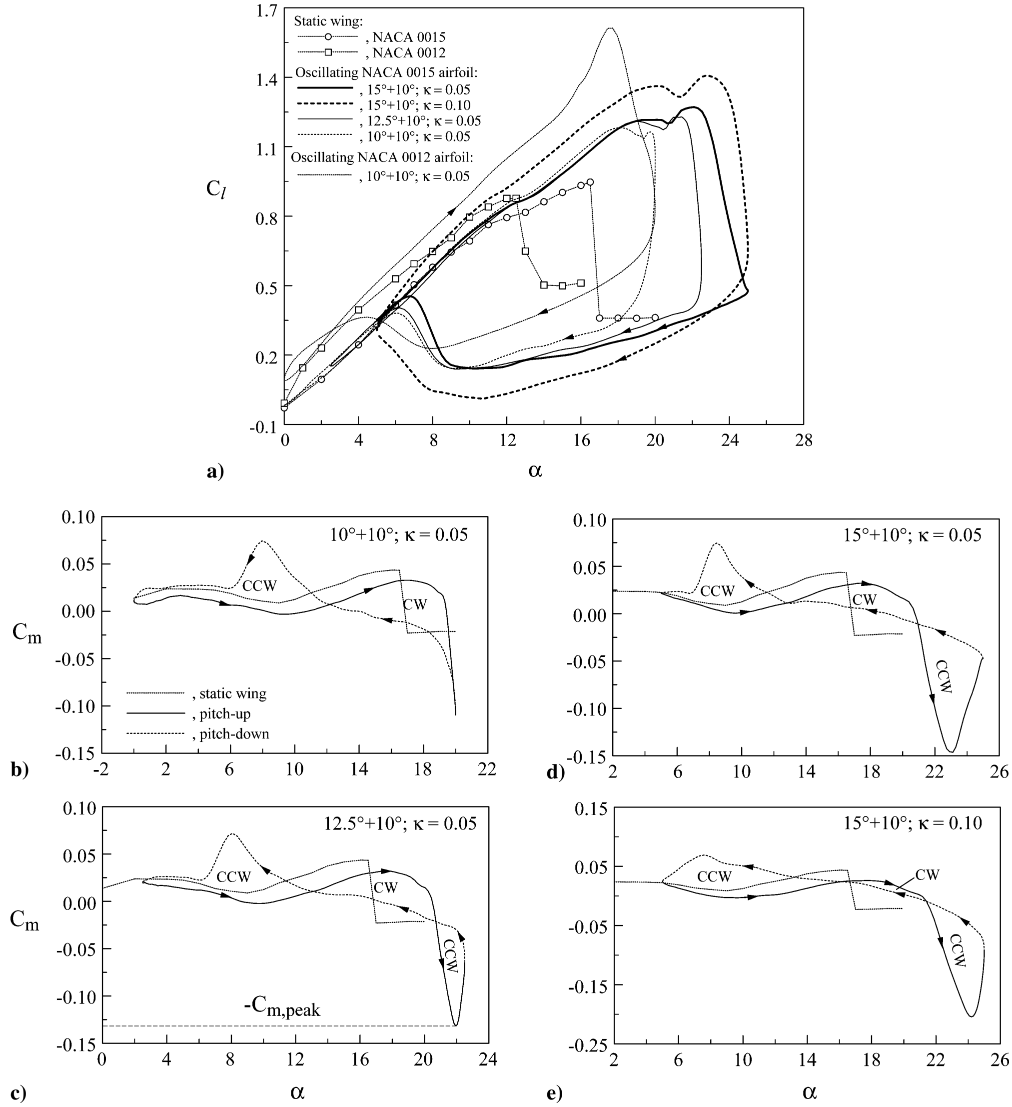

Fig. 2 Baseline-wing dynamic airloads.

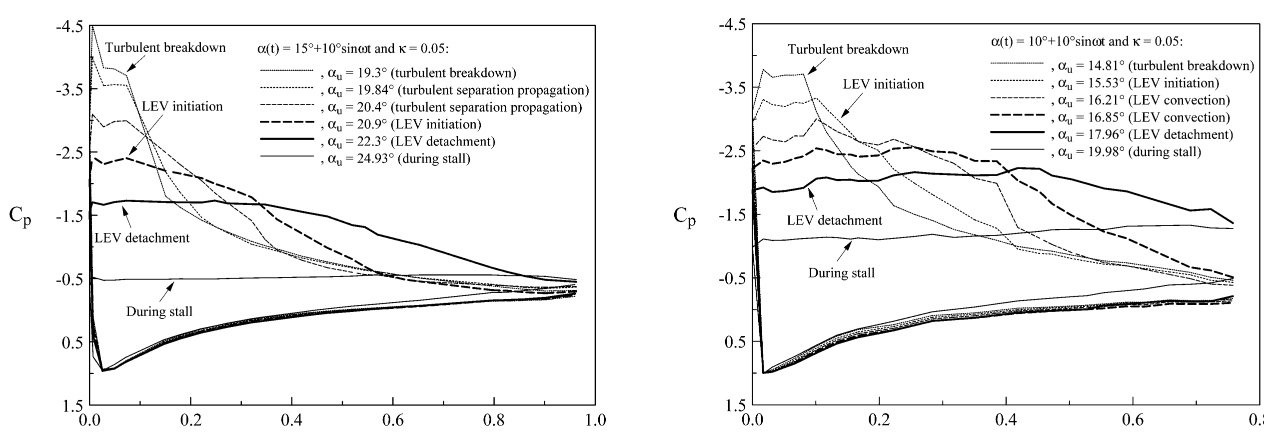

Fig. 3 Representative baseline-wing C_p distribution: a) NACA 0015 airfoil and b) NACA 0012 airfoil.

layer (at $\alpha_u = 14.8$ deg) and its rapid upstream movement, which led to an instant disruption of the laminar separation bubble and, subsequently, the initiation of the formation and convection of an energetic LEV (at $\alpha_u = 15.5$ deg). As a consequence, a single peak in C_l prior to the dynamic stall at $\alpha_{ds} = 17.7$ deg was observed. For $\kappa = 0.1$, a further increase in α_{ds}, $C_{l,\max}$, $C_{d,\max}$, and $|-C_{m,\text{peak}}|$ was observed. A detailed analysis of the behavior of the unsteady boundary-layer and stall events on an oscillating NACA 0012 airfoil is given by Lee and Gerontakos.[6] Nevertheless, more detailed on-surface measurements of the flow on the oscillating NACA 0015 airfoil are required before a definitive statement can be made.

Note that the double peaks appeared persistently in the dynamic C_l curve for an oscillating NACA 0015 airfoil, regardless of the magnitude of α_m or $\alpha_{\max}$. However, it is clear that for a NACA 0015 airfoil oscillating with different mean angles of attack α_m with the amplitude $\Delta\alpha$ fixed at 10 deg, the character of the hysteresis loop,

Table 1 Values describing flap deflection profile[a]

Case	δ, deg	t'_s	t_s	t_s, deg	t'_d	t_d	$t_d\ (f_o^{-1})$, %	t_{ss}/t_d	t'_e	t_e	t_e, deg
1	+15	47.05	-0.50π	5.0_u	35.05	1.12π	55.8	0.43	19.26	0.61π	24.4_d
2	+15	47.05	-0.50π	5.0_u	26.65	0.85π	42.7	0.23	10.98	0.35π	23.9_u
3	+15	0.00	0.00π	15.0_u	36.00	1.15π	57.3	0.41	36.00	1.15π	10.6_d
4	+15	−0.32	-0.01π	14.7_u	29.16	0.93π	46.3	0.31	28.85	0.92π	17.5_d
5	+15	0.00	0.00π	15.0_u	22.01	0.70π	35.1	0.15	22.01	0.70π	23.1_d
6	+15	14.84	0.47π	25.0_u	35.37	1.13π	56.3	0.42	−12.63	-0.40π	5.5_u
7	+15	14.84	0.47π	25.0_u	25.90	0.82π	41.2	0.18	40.74	1.30π	7.0_d
8	+15	27.91	0.89π	18.4_d	35.68	1.14π	56.8	0.43	0.94	0.03π	15.9_u
9	+15	27.91	0.89π	18.4_d	26.84	0.85π	42.7	0.19	−8.15	-0.26π	7.7_u
10	−15	47.05	-0.50π	5.0_u	32.93	1.05π	52.3	0.43	17.25	0.55π	24.9_d
11	−15	47.05	-0.50π	5.0_u	25.71	0.82π	41.2	0.25	10.03	0.32π	23.4_u
12	−15	0.63	0.02π	15.6_u	34.49	1.10π	54.8	0.41	35.12	1.12π	11.3_d
13	−15	0.63	0.02π	15.6_u	26.97	0.86π	43.2	0.23	27.60	0.88π	18.7_d
14	−15	15.79	0.50π	25.0_d	34.18	1.09π	54.3	0.41	−12.86	-0.41π	5.4_u
15	−15	15.47	0.49π	25.0_u	26.97	0.86π	43.2	0.29	42.33	1.35π	6.1_d
16	−15	29.05	0.92π	17.3_d	34.49	1.10π	54.8	0.39	0.63	0.02π	15.6_u
17	−15	29.05	0.92π	17.3_d	26.65	0.85π	42.7	0.25	−7.21	-0.23π	8.4_u
18	+7.5	−0.94	-0.03π	14.1_u	26.84	0.85π	42.7	0.52	25.71	0.82π	20.4_d
19	+7.5	16.42	0.52π	25.0_d	27.16	0.86π	43.2	0.50	43.58	1.39π	5.6_d
20	+7.5	27.28	0.87π	19.0_d	26.65	0.85π	42.7	0.52	−8.78	-0.28π	7.3_u
21	−7.5	−0.32	-0.01π	14.7_u	25.40	0.81π	40.7	0.40	25.09	0.80π	20.9_d
22	−7.5	15.79	0.50π	25.0_d	25.40	0.81π	40.7	0.49	41.08	1.31π	6.7_d
23	−7.5	32.30	1.03π	14.0_d	25.71	0.82π	41.2	0.51	−4.70	-0.15π	10.5_u

[a] $t'_s = t_s u_\infty / c$; $t'_d = t_d u_\infty / c$; 15_u deg denotes $\alpha = 15$ deg during pitch-up; $t_d = 57\%$ denotes 57% of the oscillation period; t_{ss} = steady-state time period; $t'_e = t_e u_\infty / c$; t_e denotes the end of the flap actuation duration.

particularly the pitching moment loop, changed radically as α_m was increased from 10 to 15 deg (representing the light- and deep-stall oscillations, respectively). The presence of the hysteresis was due to the fact that full flow reattachment was not obtained until the airfoil was well below its normal static stall angle, as a result of the lag induced by the reverse kinematic induced camber effect on the leading-edge pressure gradient by the negative pitch rate. The hysteresis effects were the source of reduced aerodynamic damping which can potentially lead to a variety of aeroelastic problems on the rotor. A large amount of hysteresis was present in all three C_l, C_d, and C_m components of the airloads. Figures 2b–2d clearly indicate that a progressive reduction in torsional damping (for a given $\Delta\alpha$ and κ) was apparent as α_m was decreased. Note that positive and negative contributions to the damping correspond to the counterclockwise (CCW) and clockwise (CW) loops in the C_m–α curve, respectively. The light stall introduced a second CW C_m-loop of negative damping and rendered the C_m curve a figure-eight-like behavior (Fig. 2b); a moment stall at $\alpha_{\mathrm{ms}} = 19.2$ deg slightly ahead of $\alpha_{\mathrm{ds}} = 19.8$ deg was observed. In the meantime, the $-C_{m,\mathrm{peak}}$ was found to occur at the end of the pitch-up motion. With a further increase in α_m (i.e., a deep dynamic stall case), another loop in the CCW sense was presented (Figs. 2c and 2d); a moment stall occurred earlier in the oscillation cycle, relative to the maximum angle of attack, whereas the peak nose-down pitching moment occurred while α was still increasing. In other words, more positive, or CCW, torsional damping was restored when deep stall penetration occurred (Figs. 2c and 2d). The results also show that for both light- and deep-stall oscillations, the lift stall always occurred after the moment stall. Figures 2a and 2e further indicate that higher κ further delayed the dynamic stall to a higher α with a decrease in the negative torsional damping.

B. Effect of t_d

The effects of flap duration t_d on the dynamic-load loops of a NACA 0015 airfoil oscillating with $\alpha(t) = 15\ \mathrm{deg} + 10\ \mathrm{deg}\sin\omega t$ and $\kappa = 0.05$ were investigated first with the flap actuation start time t_s and the upward deflection $\delta_{\max}$ set at 0π radian and $+15$ deg, respectively. The magnitude of $\delta_{\max} = +15$ deg (the maximum flap deflection attainable by the present TEF actuation mechanism) was chosen to best reflect the greatest reduction in $|-C_{m,\mathrm{peak}}|$ and the negative damping. Note that the upward flap deflection made the ordinates of the mean camber line negative in the trailing-edge region and affected the pitching moment. As a consequence, the zero-lift angle became more positive, and the lift and the nose-down pitching moment were reduced for a given angle of attack. The start time (corresponding to a flap actuation initiated at $\alpha_u = 15$ deg) was chosen to allow the actuation of the flap at around the onset of flow reversal during the second stage of the pitch-up motion. Details of the parameters describing the flap actuation profile in various units are given in Table 1.

Three flap actuations t_d (corresponding to 57, 46, and 35% of the oscillation cycle time period f_o^{-1}, respectively) were considered and the resulting dynamic C_l–C_d–C_m loops are displayed in Fig. 4. It is evident that, similarly to an inverted Gurney flap,[21] the upward flap deflection motions increased the effective negative camber of the airfoil, resulting in reduced overall airfoil circulation and lift. A 13% drop in $C_{l,\max}$ and a slight $\Delta\alpha_{\mathrm{ds}} \approx 0.5$ deg decrease in the dynamic stall angle, insensitive to the extent of the flap actuation duration tested, was observed (Fig. 4a), compared to a baseline wing. The poststall drop in C_l was, however, increased with increasing t_d. Note that for the TEF-controlled case, the double peaks in the C_l curve prior to the dynamic stall persisted but with the second peaked C_l value (occurred at $\alpha_{\mathrm{ds}} \approx 21.7$ deg) of a much lower magnitude than that at the first peak (at $\alpha_u \approx 18$ deg). The phase angles at which the formation, convection and detachment of the LEV was found to be virtually unaffected by the upward TEF motion. The low-pressure signature or footprint of the LEV was, however, reduced by the upward flap deflection, compared to a baseline wing (Figs. 5c and 5d). The C_p distributions are also shown three-dimensionally in Fig. 6b for $t_d = 57\% f_o^{-1}$. The presence of the LEV and flow reattachment was marked by the low-negative-pressure ridges moving downstream in the leading- and trailing-edge regions, respectively, with increasing α, as shown in Fig. 6. Special attention should be given to the presence of suction pressure on the lower surface of the flap during the flap actuation (Fig. 6b), compared to a baseline wing (Fig. 6a).

In addition, similar to the reduction observed in C_l, the upward TEF motion also led to a reduced C_d (Fig. 4b). Most importantly, the upward TEF deflection primarily provided a mitigation of the excessive nose-down C_m produced by the transient LEV effects (Figs. 4c–4e). The peak value of the negative C_m was, however, found to be insensitive to the magnitude of the flap actuation duration provided that the flap remains deflected during its occurrence. The values of the critical aerodynamic flow features for both controlled and uncontrolled TEF conditions, including the static wing, are summarized in Table 2. In summary, as can be seen from Figs. 4–6, an upward TEF deflection always led to a reduction in

Table 2 Critical unsteady aerodynamic values[a]

Case	t_s	t_d (f_o^{-1}), %	δ, deg	$C_{l,\max}$	α_{ds}	$C_{d,\max}$	α_{ms}	$C_{m,\text{peak}}$	$C_{w,\text{ccw}}$	$C_{w,\text{cw}}$	$C_{w,\text{net}}$
				NACA 0012							
Static	——	——	——	0.93	13.00	0.08	13.00	−0.039	——	——	——
10 + 10, 0.05	——	——	——	1.61	17.71	0.46	15.18	−0.157	0.55	−0.13	0.42
				NACA 0015							
Static	——	——	——	0.95	16.50	0.12	16.50	−0.023	——	——	——
15 + 10, 0.1	——	——	——	1.41	22.73	0.59	21.16	−0.204	0.74	−0.04	0.70
15 + 10, 0.05	——	——	——	1.27	22.10	0.50	20.65	−0.146	0.50	−0.14	0.36
12.5 + 10, 0.05	——	——	——	1.23	21.44	0.47	20.23	−0.132	0.38	−0.18	0.20
10 + 10, 0.05	——	——	——	1.18	19.77	0.39	19.20	−0.110	0.32	−0.25	0.07
1	-0.50π	55.8%	+15	0.93	22.53	0.39	20.90	−0.049	0.01	−1.39	−1.38
2	-0.50π	42.7%	+15	1.27	22.32	0.51	21.16	−0.152	0.27	−1.09	−0.82
3	0.00π	57.3%	+15	1.10	21.87	0.40	20.90	−0.042	0.55	−0.04	0.51
4	-0.01π	46.3%	+15	1.09	21.64	0.40	20.65	−0.040	0.39	−0.36	0.03
5	0.00π	35.1%	+15	1.10	21.64	0.40	20.65	−0.042	0.22	−0.39	−0.16
6	0.47π	56.3%	+15	1.27	22.10	0.51	20.38	−0.150	1.85	0.00	1.85
7	0.47π	41.2%	+15	1.28	21.87	0.51	20.38	−0.147	1.46	0.00	1.46
8	0.89π	56.8%	+15	1.26	22.10	0.50	20.65	−0.146	0.87	−0.08	0.79
9	0.89π	42.7%	+15	1.26	22.10	0.50	20.38	−0.148	1.21	−0.08	1.14
10	-0.50π	52.3%	−15	1.58	20.65	0.61	19.28	−0.229	2.09	0.00	2.09
11	-0.50π	41.2%	−15	1.38	20.90	0.49	19.56	−0.143	1.53	0.00	1.53
12	0.02π	54.8%	−15	1.58	21.16	0.65	19.84	−0.242	0.58	−0.01	0.57
13	0.02π	43.2%	−15	1.58	21.16	0.65	19.56	−0.248	1.04	−0.01	1.03
14	0.50π	54.3%	−15	1.26	22.10	0.50	20.38	−0.144	0.02	−1.32	−1.31
15	0.49π	43.2%	−15	1.26	22.10	0.50	20.38	−0.146	0.13	−1.05	−0.93
16	0.92π	54.8%	−15	1.26	21.87	0.50	20.38	−0.146	0.38	−0.66	−0.28
17	0.92π	42.7%	−15	1.27	22.10	0.51	20.38	−0.149	0.29	−0.84	−0.56
18	-0.03π	42.7%	+7.5	1.10	22.32	0.44	20.65	−0.098	0.34	−0.38	−0.04
19	0.52π	43.2%	+7.5	1.27	21.87	0.50	20.38	−0.149	1.12	0.00	1.12
20	0.87π	42.7%	+7.5	1.26	21.87	0.50	20.38	−0.146	1.13	−0.08	1.05
21	-0.01π	40.7%	−7.5	1.38	21.64	0.51	20.11	−0.188	0.86	−0.00	0.85
22	0.50π	40.7%	−7.5	1.26	22.10	0.50	20.65	−0.146	0.28	−0.57	−0.30
23	1.03π	41.2%	−7.5	1.25	22.10	0.50	20.38	−0.146	0.37	−0.28	0.09
24	——	——	+15	0.92	22.10	0.39	20.90	−0.039	0.30	−0.05	0.24
25	——	——	−15	1.54	20.65	0.62	19.28	−0.237	0.59	−0.15	0.44

[a]For the static cases, α_{ds} is the static stall angle and $C_{d,\max}$ is the value of C_d at the static stall angle. $C_{w,\text{CCW}}$ and $C_{w,\text{CW}}$ denote damping factors associated with counterclockwise and clockwise C_m loops, respectively.

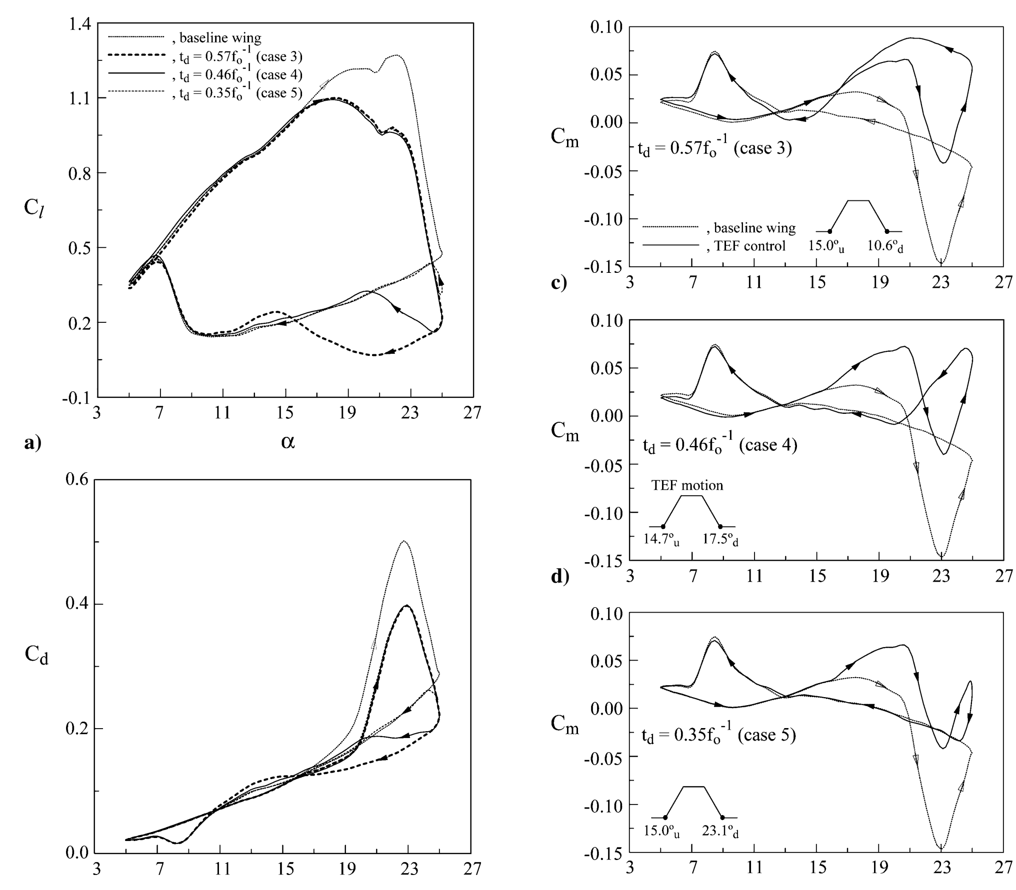

Fig. 4 Effect of flap actuation duration with $\delta_{\max}$ = +15 deg and t_s = 0π radian.

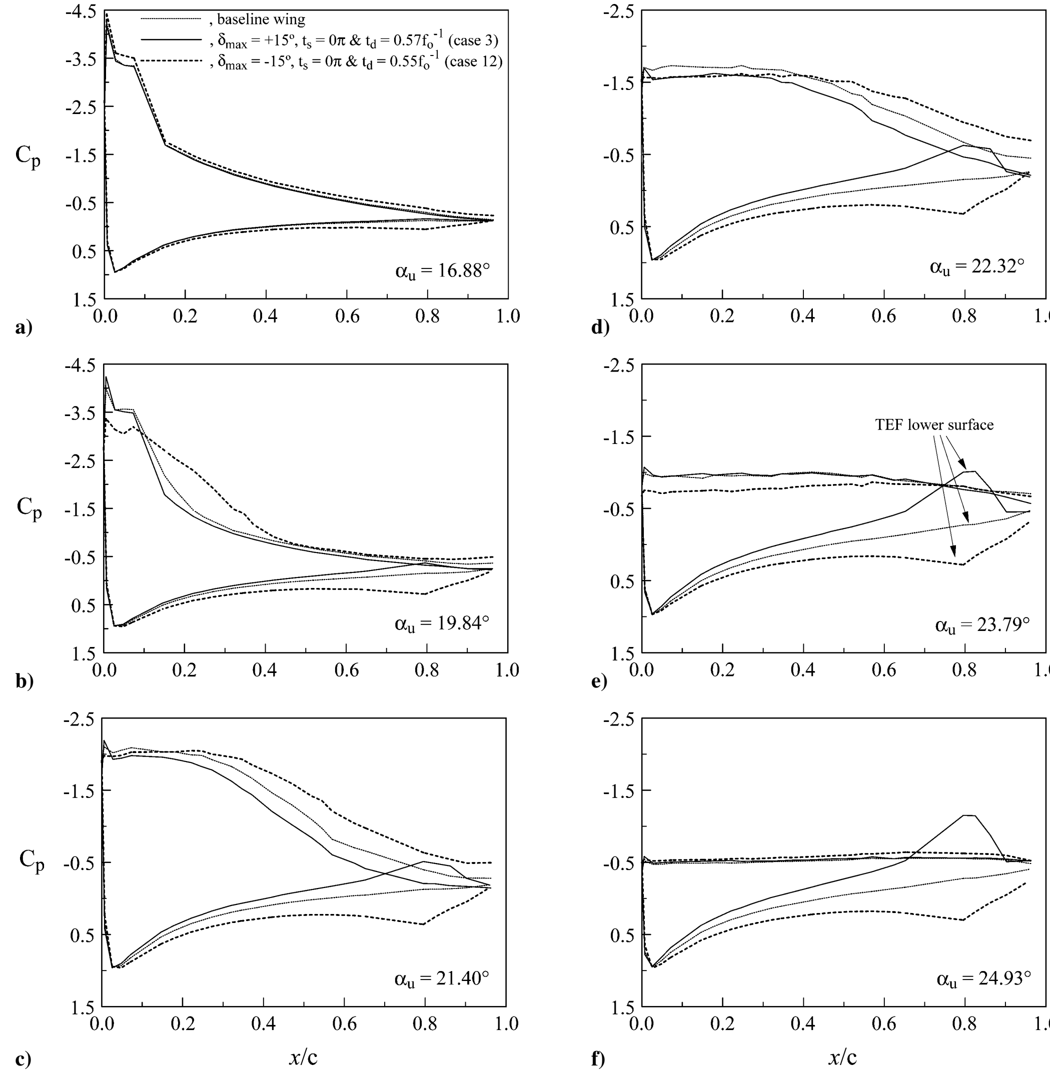

Fig. 5 Typical C_p distributions.

$C_{l,\max}$ and $C_{d,\max}$, and alleviated the large overshoot in nose-down C_m. Also, the shorter the actuation the smaller the poststall lift loss. The critical aerodynamic values were, however, found to be rather insensitive to the magnitude of t_d (Table 2).

It is also of importance to note that the underlying physics responsible for the observed decrease in lift and the peak nose-down pitching moment, as a result of the upward flap deflection, was clearly due to the fact that the pressure on the upper surface was increased, whereas the pressure was seen to decrease, in particular, on the lower surface of the flap (Fig. 5). This pressure difference contributed to the increment of the nose-up pitching moment at this stage of the flow. This phenomenon was more obvious during the LEV formation and detachment (Figs. 5b–5d) and during the during-stall flow conditions (Figs. 5e and 5f). Note that the present explanation of the observed decrease of the undesirable nose-down pitching moment, mainly as a result of the presence of suction pressure on the "lower" surface of the flap, is, however, in contrast to the mechanism suggested by Feszty et al.[11] Their computational fluid dynamics results suggest that, for a NACA 0012 airfoil oscillating with $\alpha(t) = 15$ deg $+10$ deg $\sin \omega t$ and $\kappa = 0.173$ at $Re = 1.463 \times 10^6$, the alleviation of the nose-down pitching moment was primarily attributed to the flap-introduced TEV, which caused another suction peak (in addition to the LEV-induced suction peak) over the "upper" surface of the airfoil in the trailing-edge region, and the subsequent modification of the trajectory of the LEV.

The effect of the upward TEF motion on the wake flow structure was also investigated for $t_d = 0.43 f_o^{-1}$ (i.e., with a flap actuation duration accounting for 43% of the oscillation cycle period) for which the mean and fluctuating components of the streamwise velocity are presented in Fig. 7. The upward TEF motion was efficient in containing a reduced momentum deficit throughout the oscillation cycle and resulted in a reduced drag and a generally narrowed wake width during pitch-up (Fig. 7a), accompanied by a slightly reduced streamwise velocity fluctuation (Fig. 7b). The shape of the wake profile, however, was not dramatically altered comparing to a baseline wing though its centerline was shifted upwards. No noticeable change in C_d was observed, compared to the baseline case, during pitch-down, that is, after the end of flap actuation.

Finally, a torsional damping factor was also defined by the line integral[22,23]

$$C_w = \int C_m(\alpha)\,\mathrm{d}\alpha = \int_{\mathrm{ccw}} C_m(\alpha)\,\mathrm{d}\alpha + \int_{\mathrm{cw}} C_m(\alpha)\,\mathrm{d}\alpha \qquad (1)$$

C_w is positive when it corresponds to a CCW loop while negative for a CW loop in the C_m vs α curve. The positive $C_{w,\mathrm{ccw}}$ and negative $C_{w,\mathrm{cw}}$ torsional damping factors and the net $C_{w,\mathrm{net}}$ value for the three t_d tested are summarized in Table 2. Table 2 clearly shows that for cases 3–5 the longest $t_d = 0.57 f_o^{-1}$ flap actuation provided a situation with significantly improved torsional aerodynamic damping (i.e., decreased negative damping), compared to a baseline wing.

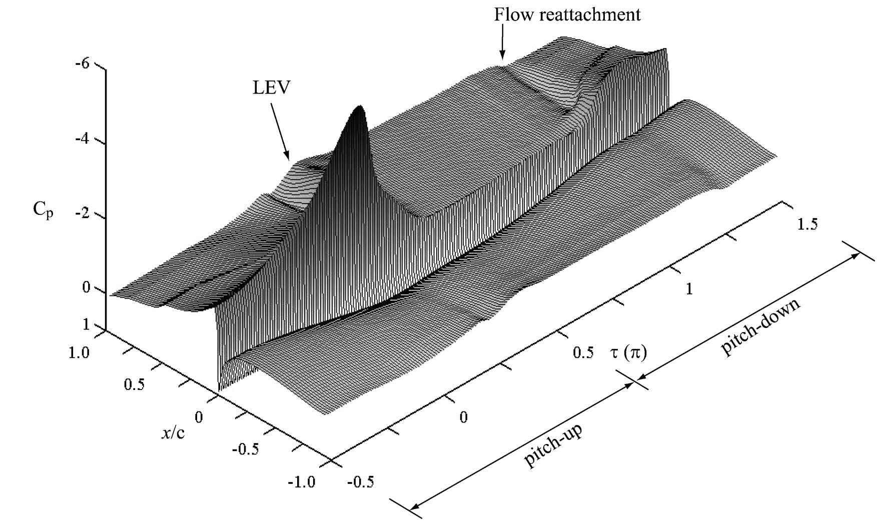

a) Baseline wing

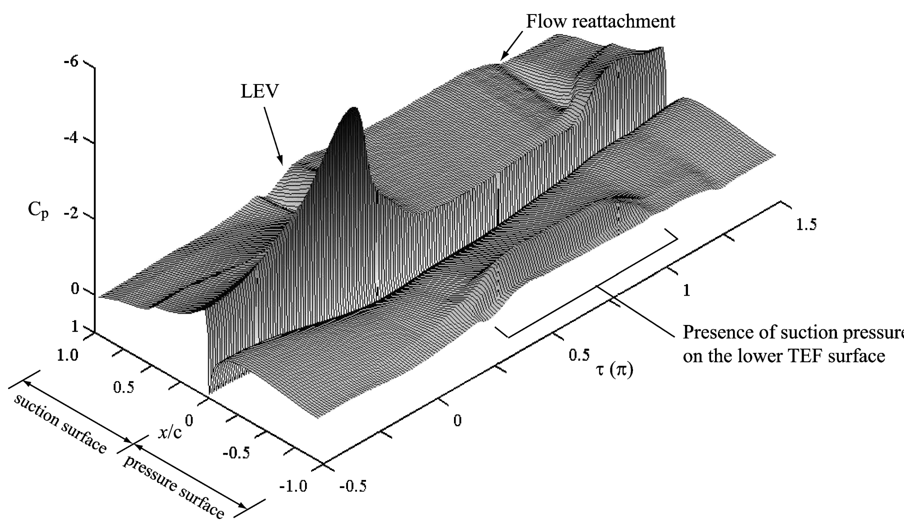

b) $\delta_{\max}$ = +15 deg, t_s = 0π and t_d = 0.57f_o^{-1} (case 3)

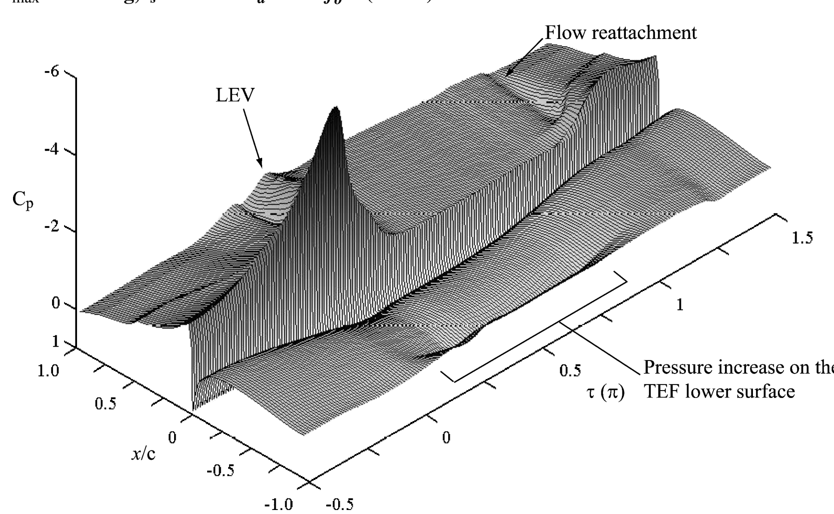

c) $\delta_{\max}$ = −15 deg, t_s = 0.02π and t_d = 0.55f_o^{-1} (case 12)

Fig. 6 Typical three-dimensional representation of C_p distribution.

C. Effect of t_s

The effects of the flap actuation start time t_s on the dynamic load loops were investigated with t_d and $\delta_{\max}$ fixed at about $0.57 f_o^{-1}$ and $+15$ deg, respectively. Four different t_s (-0.5π, 0π, 0.47π, and 0.89π radians corresponding to a flap actuation initiated at 5_u, 15_u, 25_u, and 18.4_d deg, respectively) were tested (Fig. 8); 15_u deg and 18.4_d deg denote $\alpha_u = 15$ deg and $\alpha_d = 18.4$ deg during pitch-up and pitch-down, respectively. As can be seen, although earlier actuations reduced the peak nose-down pitching moment more effectively, they also led to significant loss in the maximum achievable dynamic lift. The $t_s = -0.5\pi$ case (with $t_d = 0.56 f_o^{-1}$), representing an upward flap deflection covering the entire upstroke motion, basically acted like an inverted Gurney flap shifting the lift-curve vertically downward during pitch-up and, consequently, rendered a dramatic reduction in $C_{l,\max}$ and $|-C_{m,\text{peak}}|$. The value of $C_{w,\text{net}}$ was, however, decreased considerably (i.e., a substantially increased

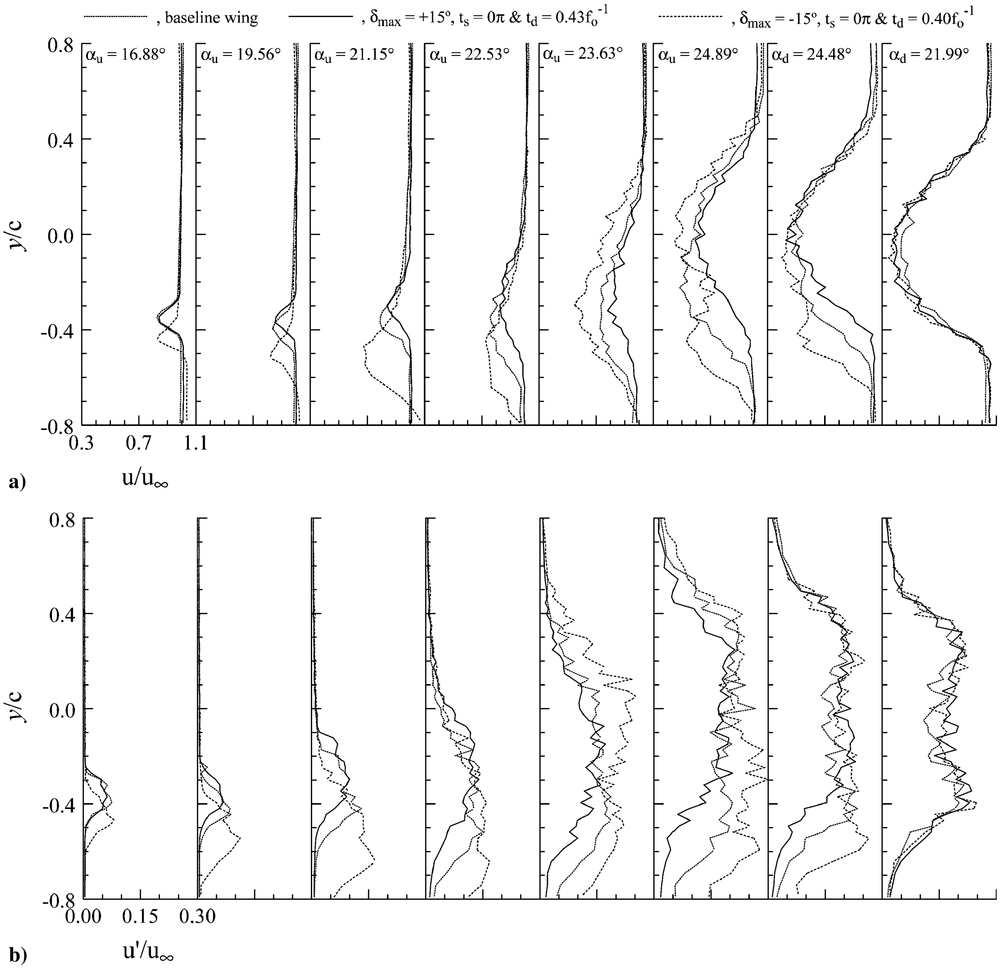

Fig. 7 Typical wake velocity profiles.

negative damping, Table 2), as a result of the presence of the large CW loop in the C_m–α curve (Fig. 8b). The differences in C_l, C_d, and C_m between the controlled and uncontrolled cases can also be readily illustrated by plotting ΔC_l, ΔC_d, and ΔC_m against the flap actuation profiles (Fig. 9). Figure 9 clearly indicates that the upward flap deflection always produced a significant increase in the value of C_m and a decrease in C_l, compared to a baseline wing. Depending on the magnitude of t_s, a relatively small improvement in C_d was observed. More importantly, the occurrence of the LEV and the promotion of the flow reattachment can also be directly identified from the dips shown in the ΔC_l, ΔC_d, and ΔC_m curves. Note that for an uncontrolled baseline wing the flow reattachment was found to occur at around $\alpha_d = 9$ deg.

Figure 8 also shows that for TEF deflection actuated during pitch-down (i.e., $t_s = 0.47\pi$ and 0.89π TEF control cases), the C_l curve remained unchanged during pitch-up, compared to a baseline wing, while the poststall lift loss and the hysteresis were found to increase with increasing t_s. It is interesting to note that although the value of $-C_{m,\text{peak}}$ was not affected, there was a reduction in the positive $C_{w,\text{net}}$ value in the case of the highest t_s. Noteably, this is contrary to the trend in $C_{w,\text{net}}$ for the other values of t_s (Table 2). The variation of the critical aerodynamic performance and C_w values with t_s, t_d, and $\delta_{\max}$ are summarized in Table 2 and Fig. 10.

D. Effect of $\delta_{\max}$

The effects of flap deflection amplitude $\delta_{\max}(-15$ and ± 7.5 deg) on the dynamic C_l and C_m curves was investigated at fixed t_s and t_d. Figure 11 shows that for downward flap deflection $\delta_{\max} = -15$ deg with $t_d \approx 0.54 f_o^{-1}$ and $t_s = -0.5\pi$–0.92π (corresponding to a flap actuated in the first, second, and third quarter of the azimuth, respectively), the separation on the suction surface of the airfoil was suppressed, especially in the trailing-edge region, to higher angles of attack. That is, dynamic downward TEF deflection (actuated during pitch-up at $t_s = -0.5\pi$ and 0.02π or at $\alpha_u = 5$ and 15.6 deg, respectively) led to a drastic suppression of the boundary-layer thickness in the vicinity of the trailing edge and also assured attached flow over the suction surface of the airfoil to the highest possible angle of attack. The downward TEF motion-induced positive effective camber effects, similar to those of a Gurney flap[21] shifted the lift-curve upward and caused a considerable increase in $C_{l,\max}$, although the α at which the $C_{l,\max}$ occurred was slightly decreased (Fig. 11a). Note that for a wing with a Gurney flap the stagnation moved to the lower surface of the airfoil. Also, the streamlines were deflected upward in the vicinity of the leading edge and downward near the trailing edge by deflecting the flap downward. Figure 11b also shows that, as expected, the increase in C_l and $C_{l,\max}$ was accompanied by a substantially intensified peak nose-down pitching moment, as shown in Figs. 11b and 11c (for $t_s = -0.5\pi$ and 0.02π), compared to a baseline wing. The $C_{w,\text{net}}$ value, however, were found to be positive and were higher than a baseline wing (see Table 2 and Fig. 10). It is also significant to note that the downward flap deflection also translates into an increase in suction pressure on the upper wing surface, as well as a significant increase in the pressure on the pressure surface (Figs. 5 and 6), in contrast to an upward flap deflection, compared to a baseline wing. Considerable increase in the hysteresis in the lift curve was observed for the $t_s = -0.5\pi$ case.

Figure 11 also shows that for flap actuations began during the early stage of the pitch-down motion (i.e., $t_s = 0.5\pi$ and 0.92π), the $C_{l,\max}$ and α_{ds} values were not affected, and that there was a poststall lift improvement that led to a reduced hysteresis. The magnitude of $-C_{m,\text{peak}}$ remained unchanged, whereas the $C_{w,\text{net}}$ became negative. The later the actuation the smaller and more negative the net torsional damping was, except for the latest actuation time for which $C_{w,\text{net}}$, although still negative, increased compared to the $t_s = 0.5\pi$

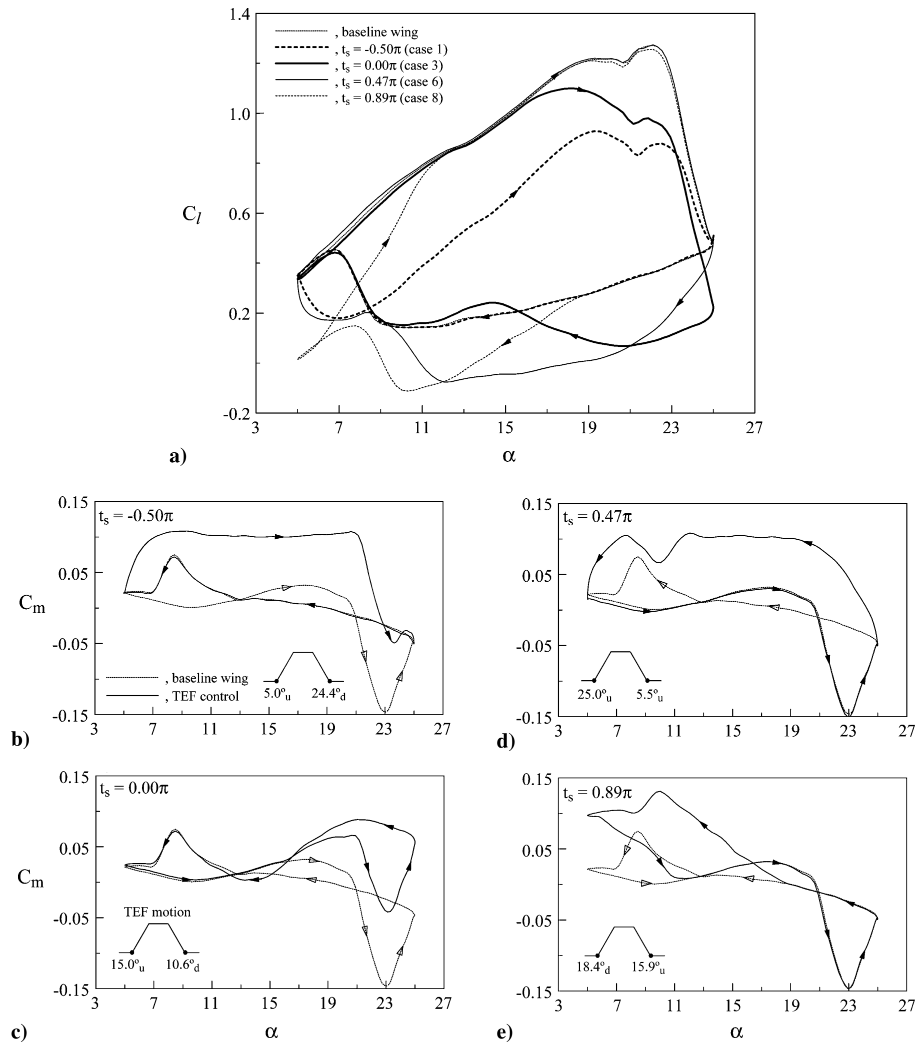

Fig. 8 Effect of flap actuation start time with $\delta_{\max}$ = +15 deg and $t_d \approx 0.57 f_o^{-1}$.

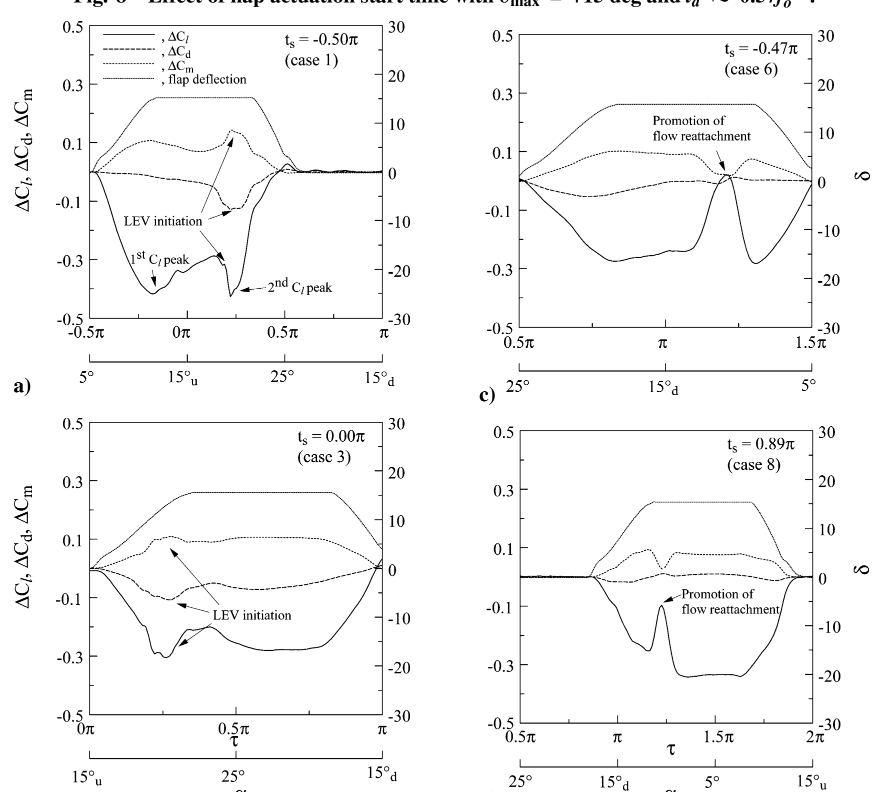

Fig. 9 Variation of ΔC_l, ΔC_d, and ΔC_m for $\delta_{\max}$ = +15 deg and $t_d = \approx 0.57 f_o^{-1}$.

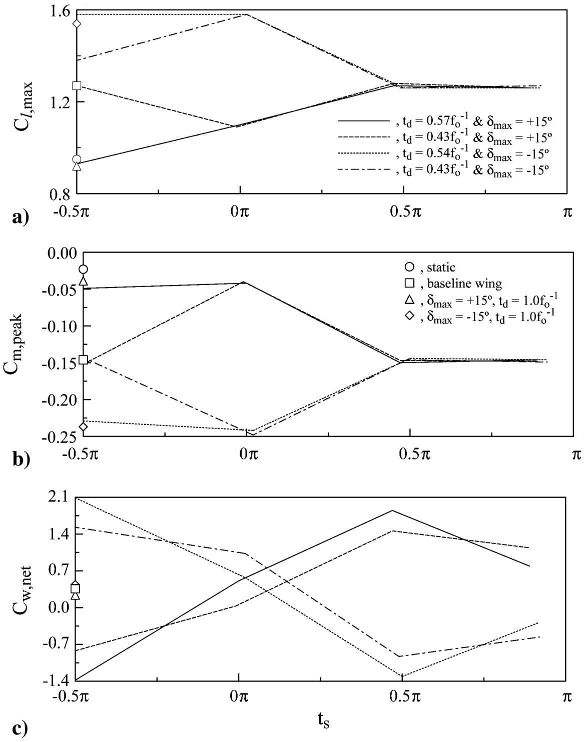

Fig. 10 Variation of $C_{l,\max}$, $C_{m,\mathrm{peak}}$, and C_w with TEF motion.

case (Fig. 11 and Table 2). Moreover, for a downward flap deflection the overall pitch-down flow reattachment process was found to be insensitive to the magnitude of t_s. The effects of the downward flap deflection can also be depicted from the typical mean and fluctuating wake velocity profiles for $\delta_{\max} = -15$ deg, $t_s = 0\pi$, and $t_d = 0.40 f_o^{-1}$ (Fig. 7). Figure 7 clearly indicates that the increase in C_l, C_d, and $|-C_{m,\mathrm{peak}}|$ was accompanied by an increased wake width, wake deficit, as well as increased velocity fluctuations, and shifted the wake centerline downward.

IV. Conclusions

The control of the dynamic stall flow over a NACA 0015 airfoil oscillated with $\alpha(t) = 15$ deg $+10$ deg $\sin \omega t$ and $\kappa = 0.05$ at $Re = 1.65 \times 10^5$, via a movable trailing-edge flap, was investigated through surface pressure measurements, supplemented by cross-hot-wire wake-flow data. Both upward and downward flap deflections at different flap actuation start times and durations were considered. Key TEF control features are drawn: 1) only upward flap deflections led to the reduction of negative $C_{m,\mathrm{peak}}$; 2) the larger the flap deflection the more efficient the reduction mechanism was; 3) the shorter the actuation duration the smaller the poststall lift loss; 4) the magnitudes of $C_{l,\max}$ and $C_{d,\max}$ seemed to be somewhat insensitive to the extent of flap actuation duration but were of lower values than a baseline wing; 5) the later the t_s the larger the $C_{w,\mathrm{net}}$, in general; and 6) the LEV formation and detachment were not affected by the TEF motion, whereas the low-pressure signature or footprint of the LEV was reduced by the upward flap deflection. More importantly, the reduction in $|-C_{m,\mathrm{peak}}|$ was found to be a consequence of the suction pressure introduced on the lower surface of the control

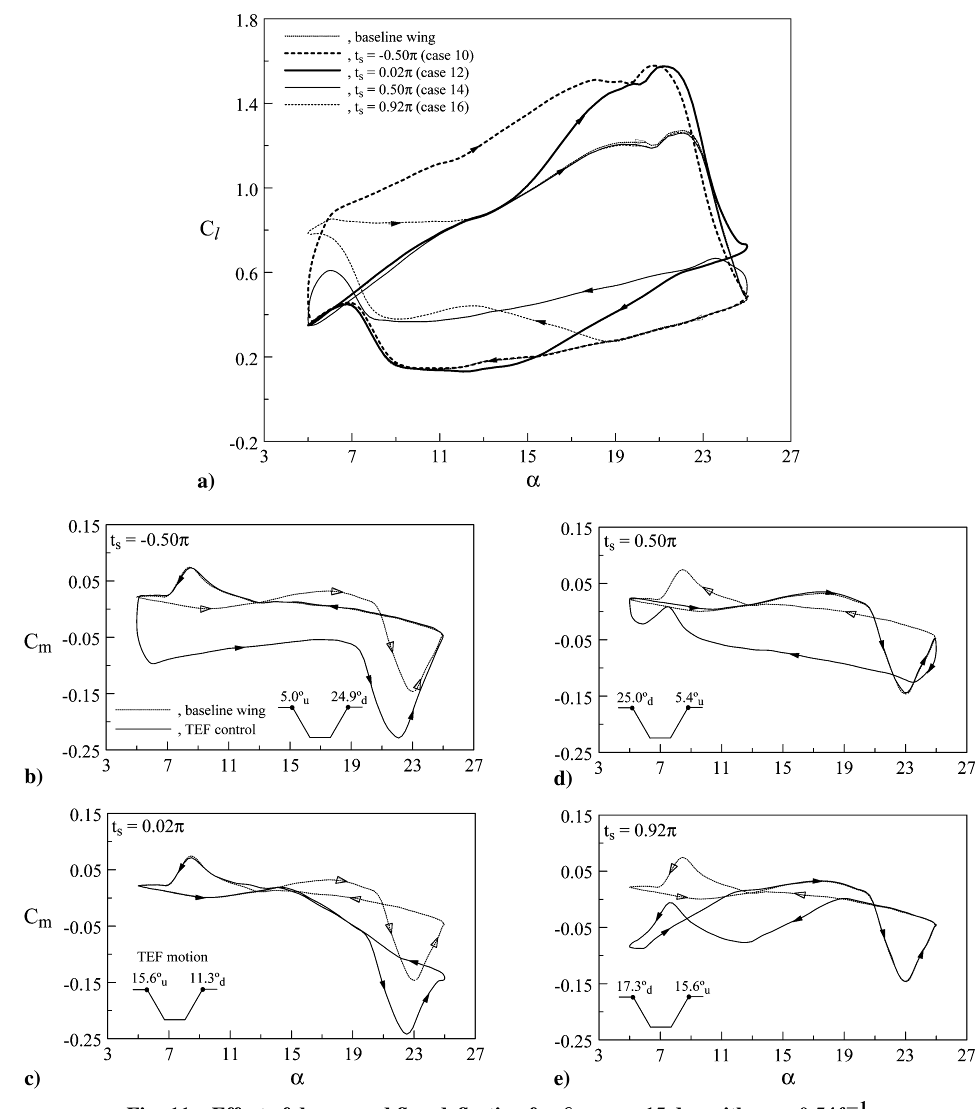

Fig. 11 Effect of downward flap deflection for $\delta_{\max} = -15$ deg with $t_d \approx 0.54 f_o^{-1}$.

flap. In conclusion, a relatively early flap actuation (initiated between α_{ss} and α_{max} during pitch-up, i.e., during the latter part of the second quarter of the azimuth) and a rather long duration (about half of the oscillation cycle time), in conjunction with an upward flap deflection (with $\delta_{max} \geq 60\%\alpha_{max}$), should be more effective in reducing the nose-down pitching moment excursion, and in providing a good compromise between negative damping and maximizing dynamic lift. However, implementation of a closed-loop control system is needed. Finally, both off- and on-surface flow measurements and visualizations are needed to better understand the phenomena reported here.

Acknowledgments

This work was supported by the Natural Science and Engineering Research Council of Canada. D. Birch is thanked for the design and construction of the trailing-edge flap control system.

References

[1]McCroskey, W. J., Carr, L. W., and McAlister, K. W., "Dynamic Stall Experiments on Oscillating Airfoils," *AIAA Journal*, Vol. 14, No. 1, 1976, pp. 57–63.

[2]Carr, L. W., McAlister, K. W., and McCroskey, W. J., "Analysis of the Development of Dynamic Stall Based on Oscillating Airfoil Experiments," NASA TN D-8382, Jan. 1977.

[3]McCroskey, W. J., "Unsteady Airfoils," *Annual Review of Fluid Mechanics*, Vol. 14, Jan. 1982, pp. 285–311.

[4]Ericsson, L. E., and Reding, J. P., "Fluid Mechanics of Dynamic Stall. I. Unsteady Flow Concepts," *Journal of Fluids and Structures*, Vol. 2, No. 1, 1988, pp. 1–33.

[5]Lee, T., and Basu, S., "Measurement of Unsteady Boundary Layer Developed on an Oscillating Airfoil Using Multiple Hot-Film Sensors," *Experiments in Fluids*, Vol. 25, No. 2, 1998, pp. 108–117.

[6]Lee, T., and Gerontakos, P., "Investigation of Flow over an Oscillating Airfoil," *Journal of Fluid Mechanics*, Vol. 512, Aug. 2004, pp. 313–341.

[7]Rennie, R., and Jumper, E. J., "Experimental Measurements of Dynamic Control Surface Effectiveness," *Journal of Aircraft*, Vol. 33, No. 5, 1996, pp. 880–887.

[8]Vipperman, J. S., Clark, R. L., Conner, M., and Dowell, E. H., "Experimental Active Control of a Typical Section Using a Trailing-Edge Flap," *Journal of Aircraft*, Vol. 35, No. 2, 1998, pp. 224–229.

[9]Nguyen, K., "Active Control of Helicopter Blade Stall," *Journal of Aircraft*, Vol. 35, No. 1, 1998, pp. 91–98.

[10]Ekaterinaris, J. A., "Numerical Investigations of Dynamic Stall Active Control for Incompressible and Compressible Flows," *Journal of Aircraft*, Vol. 39, No. 1, 2002, pp. 71–78.

[11]Feszty, D., Gillies, E. A., and Vezza, M., "Alleviation of Airfoil Dynamic Stall Moments via Trailing-Edge-Flap Flow Control," *AIAA Journal*, Vol. 42, No. 1, 2004, pp. 17–25.

[12]Smith, B. L., and Glezer, A., "The Formation and Evolution of Synthetic Jets," *Physics of Fluids*, Vol. 10, No. 9, 1998, pp. 2281–2297.

[13]Lorber, P. F., Carta, F. O., and Carlson, R. G., "The Aerodynamics of an Oscillating Jet Flap," *Journal of the American Helicopter Society*, Vol. 34, No. 2, 1989, pp. 24–32.

[14]Greenbaltt, D., and Wygnanski, I., "Dynamic Stall Control by Periodic Excitation, 1: NACA 0015 Parametric Study," *Journal of Aircraft*, Vol. 38, No. 3, 2001, pp. 430–438.

[15]Karim, M. A., and Acharya, M., "Suppression of Dynamic-Stall Vortices over Pitching Airfoils by Leading-Edge Suction," *AIAA Journal*, Vol. 32, No. 8, 1994, pp. 1647–1655.

[16]Yu, Y. H., Lee, S., McAlister, K. W., Tung, C., and Wang, C. M., "Dynamic Stall Control for Advanced Rotorcraft Application," *AIAA Journal*, Vol. 33, No. 2, 1995, pp. 289–295.

[17]Freymuth, P., Jackson, S., and Bank, W., "Toward Dynamic Separation Without Dynamic Stall," *Experiments in Fluids*, Vol. 7, No. 3, 1989, pp. 187–196.

[18]Chandrasekhara, M. S., Wilder, M. C., and Carr, L. W., "Unsteady Stall Control Using Dynamically Deforming Airfoils," *AIAA Journal*, Vol. 36, No. 10, 1998, pp. 1792–1800.

[19]Martin, P. B., McAlister, K. W., Chandrasekhara, M. S., and Geissler, W., "Dynamic Stall Measurements and Computations for a VR-12 Airfoil with a Variable Droop Leading Edge," *Proceedings of the American Helicopter Society 59th Annual Forum*, American Helicopter Society, Alexandria, VA, 2003.

[20]Theodorsen, T., "General Theory of Aerodynamic Instability and the Mechanism of Flutter," NACA TR496, 1935.

[21]Gerontakos, P., and Lee, T., "Oscillating Wing Loadings with Trailing-Edge Strips," *Journal of Aircraft* (to be published).

[22]Carta, F. O., "An Analysis of the Stall Flutter Instability of Helicopter Rotor Blades," *Journal of American Helicopter Society*, Vol. 12, No. 4, 1967, pp. 1–18.

[23]Leishman, J. G., *Principles of Helicopter Aerodynamics*, Cambridge Univ. Press, New York, 2002, pp. 379–389.

W. Ng
Associate Editor